An Extended-Speed Low-Ripple Torque Control of Switched Reluctance Motor Drives

Jin Ye, *Student Member, IEEE*, Berker Bilgin, *Member, IEEE*, and Ali Emadi, *Fellow, IEEE*

***Abstract*—In this paper, an extended-speed low-ripple torque control of switched reluctance motor (SRM) drives using torque sharing function (TSF) is proposed. Two operational modes are defined for the online TSF during commutation: In Mode I, absolute value of rate of change of flux linkage (ARCFL) of incoming phase is higher than outgoing phase; in Mode II, ARCFL of outgoing phase is higher than incoming phase. In order to compensate the torque error produced by imperfect tracking of phase current, a proportional and integral compensator with torque error is added to the torque reference of outgoing phase in Mode I and incoming phase in Mode II. Therefore, the total torque is determined by the phase with lower ARCFL rather than the phase with higher ARCFL as in conventional TSFs. The maximum torque-ripple-free speed of the proposed TSF is increased to more than ten times as the best case in conventional TSFs. Finally, the proposed TSF is verified by both simulations and experiments with a 2.3 kW, 6000 rpm, three-phase 12/8 SRM operating in both linear magnetic and saturated magnetic regions. Results show that the proposed TSF has higher average torque, and much lower torque ripples compared to conventional TSFs.**

***Index Terms*—Efficiency, online torque control, switched reluctance motor (SRM), torque ripple reduction, torque sharing function (TSF).**

I. Introduction

SWITCHED reluctance motor (SRM) emerges as a promising candidate in automotive applications due to the absence of windings in the rotor, four-quadrant operation, and extended-speed constant-power range [1]–[14]. However, the major drawbacks of SRM are high torque ripple, acoustic noise and vibration compared with conventional electric machine drives. Torque ripples of SRM can be reduced by several approaches [15]–[20]. In [18], torque ripple is reduced through both the machine design and control methods. In [19], a novel Lyapunov function-based direct torque control is presented to reduce the torque ripples based on nonlinear model of SRM. In [20], the optimal turn-on and turn-off angles are selected to reduce the commutation torque ripples considering nonlinearity of SRM.

Torque sharing function (TSF) [21]–[29] is gaining interest in the areas of the torque ripple reduction in SRM drives. The total torque reference is intelligently divided to each phase and the torque introduced by each phase tracks its reference defined by the TSF. Then the reference phase current is obtained according to the torque-current-rotor position characteristics. Linear, cubic, and exponential TSF are among the most frequently used ones. The actual torque output of TSF is determined by the tracking performance of each phase. As the speed of SRM increases, phase current is not able to track the reference during high speed due to the limited dc-link voltage and, therefore, torque ripples are increased.

One important evaluation criterion for TSF is the maximum absolute value of rate of change of flux linkage (ARCFL) with respect to rotor position, which should be minimized to extend the torque-speed range. The other evaluation criterion is copper loss, which should be minimized to improve efficiency of SRM drives. The selection of TSF is more challenging considering both torque-speed range and efficiency. Different selection methods for TSF are studied according to these two criteria. In [24], conventional TSFs including linear TSF, cubic TSF, sinusoidal TSF, and exponential TSF are evaluated in terms of the maximum ARCFL and copper loss. The turn-on and overlap angles are optimized by using the genetic algorithm and the best TSF is selected among four listed TSFs. In [25], a family of optimal TSFs is presented to minimize the torque ripples of SRM by using optimization method. In [26], a nonlinear logical TSF for torque ripple reduction and efficiency enhancement is introduced. Compared with the other TSFs, the logical TSF is online and not fixed. Only incoming phase or outgoing phase torque is changed and the other phase is kept the same within current limit of the motor. Therefore, only incoming or outgoing phase produces torque ripples and the total torque ripples may be reduced. However, theoretical analysis of the maximum ARCFL of logical TSF has not been provided in this paper. In [27] and [28], an iterative learning controller is proposed to add a compensation current to the current reference to reduce the torque ripple resulting from nonlinearity of SRM. In [29], adaptive TSF is presented to enhance torque–speed capability. The turn-on angle of TSF is adjusted according to operational speed. However, the shape of TSF is not adjusted and thus the torque–speed performance improvement is still limited.

In this paper, an extended-speed low-ripple torque control of SRM drives using TSF is proposed. ARCFLs of incoming phase and outgoing phase for conventional TSFs including linear, cubic, exponential TSFs are compared. The comparison results show that ARCFL of incoming phase for conventional TSFs is a little higher at the start of commutation and the ARCFL of the outgoing phase becomes much higher as commutation ends. Based on this fact, the operation of SRM is divided into two modes: In mode I, ARCFL of incoming phase is higher than

Manuscript received October 23, 2013; revised December 21, 2013, February 13, 2014, and March 29, 2014; accepted March 31, 2014. Date of publication April 14, 2014; date of current version October 15, 2014. Recommended for publication by Associate Editor J. O. Ojo.

The authors are with the McMaster Institute for Automotive Research and Technology, McMaster University, Hamilton, ON L8S 4K1 Canada (e-mail: yej25@mcmaster.ca; bilginb@mcmaster.ca; emadi@mcmaster.ca).

Color versions of one or more of the figures in this paper are available online at http://ieeexplore.ieee.org.

Digital Object Identifier 10.1109/TPEL.2014.2316272

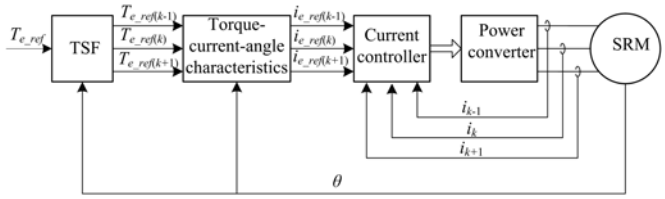

Fig. 1. Torque control diagram of SRM.

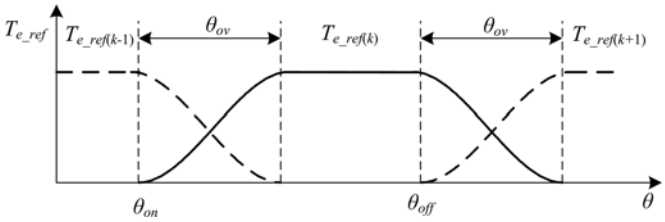

Fig. 2. Illustration of a TSF.

outgoing phase, while in mode II, ARCFL of outgoing phase is higher than incoming phase. The online torque control based on TSF is realized by using a proportional and integral (PI) compensator with the error between the torque reference and estimated torque. The output of PI compensator is added to the torque reference of the phase which has lower ARCFL, that is, the outgoing phase in Mode I and incoming phase in Mode II. Therefore, the maximum torque-ripple-free speed (TRFS) of the proposed online TSF is dependent on the phase which has lower ARCFL rather than higher ARCFL in conventional TSFs. Torque–speed performance of online TSF is greatly improved. In addition, torque expression in terms of rotor position and current are derived in both linear and saturated region of SRM and the proposed online TSF is applied to nonlinear region of SRM. Finally, the performance of conventional TSFs and the proposed online TSF are compared in terms of torque ripple, average torque and copper loss the wide speed range through simulations and experiments with a 2.3 kW, 6000 rpm, three-phase 12/8 SRM.

II. Torque Sharing Function

A. Torque Control of SRM

The torque control diagram of SRM based on TSF is shown in Fig. 1. The torque reference of each phase is defined by TSF. Neglecting the saturation and mutual flux coupling of SRM, electromagnetic torque of kth phase is derived as (1). Then phase current reference is derived according to this equation. The phase current is controlled by hysteresis controller

$$T_{e(k)}(\theta, i) = \frac{1}{2}\frac{\partial L(\theta, i_k)}{\partial \theta} i_k^2 \tag{1}$$

where $T_{e(k)}$ is the torque produced by kth phase, θ is the rotor position, $L(\theta, i_k)$ is the kth phase inductance, and i_k is the kth phase current.

The illustration of TSF in a three-phase SRM is shown in Fig. 2. The torque reference of incoming phase is rising to torque reference, and the torque reference of outgoing phase decreases to zero during commutation.

The torque reference of kth phase is defined as

$$T_{e\_\mathrm{ref}(k)} = \begin{cases} 0 & 0 \le \theta < \theta_{\mathrm{on}} \\ T_{e\_\mathrm{ref}} f_{\mathrm{rise}}(\theta) & \theta_{\mathrm{on}} \le \theta < \theta_{\mathrm{on}} + \theta_{ov} \\ T_{e\_\mathrm{ref}} & \theta_{\mathrm{on}} + \theta_{ov} \le \theta < \theta_{\mathrm{off}} \\ T_{e\_\mathrm{ref}} f_{\mathrm{fall}}(\theta) & \theta_{\mathrm{off}} \le \theta < \theta_{\mathrm{off}} + \theta_{ov} \\ 0 & \theta_{\mathrm{off}} + \theta_{ov} \le \theta \le \theta_p \end{cases} \tag{2}$$

where $T_{e\_\mathrm{ref}(k)}$ is the reference torque for kth phase, T_{e_ref} is the total torque reference, $f_{\mathrm{rise}}(\theta)$ is the rising TSF for the incoming phase, $f_{\mathrm{fall}}(\theta)$ is the decreasing TSF for the outgoing phase, and θ_{on}, θ_{off}, θ_{ov}, and θ_p are turn-on angle, turn-off angle, overlapping angle, and pole pitch, respectively.

Pole pitch is defined in (3) as a function of the number of rotor poles N_p

$$\theta_p = \frac{2\pi}{N_p}. \tag{3}$$

The sum of torque reference for incoming phase and outgoing phase is the total torque reference, and thus relationship between rising TSF and decreasing TSF can be obtained as

$$f_{\mathrm{fall}}(\theta) = 1 - f_{\mathrm{rise}}(\theta + \theta_{\mathrm{on}} - \theta_{\mathrm{off}}). \tag{4}$$

B. Conventional TSFs

The conventional TSFs including linear, cubic, and exponential TSF [24] are described in this section. Linear TSF, cubic TSF, and exponential TSF can be represented as

$$f_{\mathrm{rise}}(\theta) = \frac{1}{\theta_{ov}}(\theta - \theta_{\mathrm{on}}) \tag{5}$$

$$f_{\mathrm{rise}}(\theta) = \frac{3}{\theta_{ov}^2}(\theta - \theta_{\mathrm{on}})^2 - \frac{2}{\theta_{ov}^3}(\theta - \theta_{\mathrm{on}})^3 \tag{6}$$

$$f_{\mathrm{rise}}(\theta) = 1 - \exp\left(\frac{-(\theta - \theta_{\mathrm{on}})^2}{\theta_{ov}}\right). \tag{7}$$

C. Evaluation Criteria of TSF

In order to evaluate the torque–speed performance and efficiency of TSFs, two criteria are defined as follows.

1) The maximum ARCFL with respect to rotor position.

The maximum ARCFL M_λ is defined as (8) to evaluate the torque–speed performance of a specific TSF

$$M_\lambda = \max\left\{\left|\frac{d\lambda_{\mathrm{rise}}}{d\theta}\right|, \left|\frac{d\lambda_{\mathrm{fall}}}{d\theta}\right|\right\} \tag{8}$$

where λ_{rise} is the flux linkage for the incoming phase, λ_{fall} is the flux linkage for the outgoing phase.

The voltage equation of SRM can be derived as (9) by neglecting the mutual flux coupling

$$v = Ri + \frac{d\lambda(\theta, i)}{dt} \tag{9}$$

where v is phase voltage, i is phase current, R is resistance of winding, and λ is flux linkage.

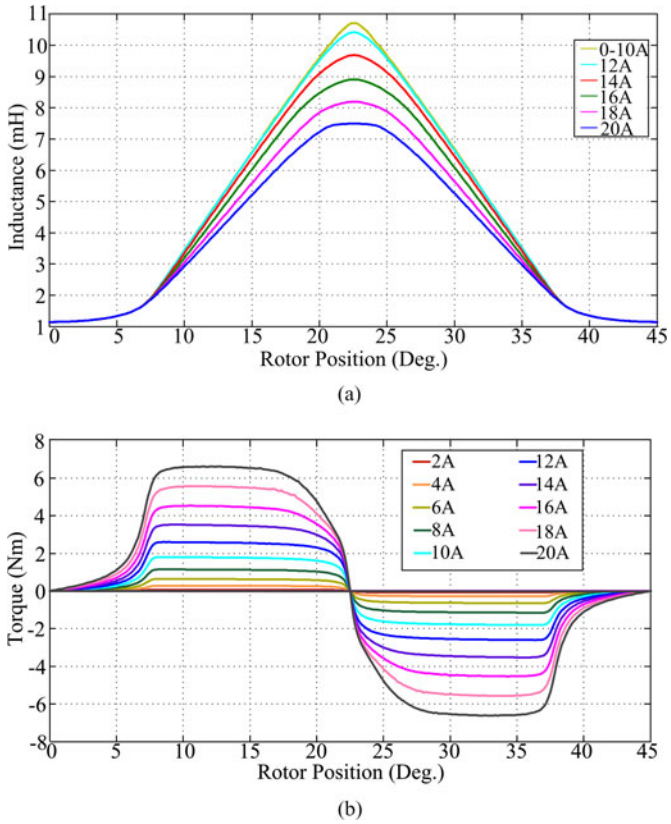

Fig. 3. FEA inductance and torque profiles of 12/8 SRM. (a) Inductance profiles. (b) Torque profiles.

The maximum TRFS is derived as (10). The ARCFL should be minimized to maximize TRFS region

$$\omega_{\max} = \frac{V_{\rm dc}}{M_\lambda} \tag{10}$$

where $\omega_{\max}$ is the maximum TRFS, and $V_{\rm dc}$ is the dc-link voltage.

2) Copper loss of electric machine.

Copper loss is an important factor influencing efficiency of the electric machine. RMS current is derived as

$$I_{\rm rms} = \sqrt{\frac{1}{\theta_p}\left(\int_{\theta_{\rm on}}^{\theta_{\rm off}} i_k^2 d\theta + \int_{\theta_{\rm on}}^{\theta_{\rm off}} i_{k-1}^2 d\theta\right)}. \tag{11}$$

III. Proposed Online TSF

A. Comparison of ARCFL of Conventional TSFs

ARCFL of incoming phase and outgoing phase for conventional TSFs including linear, cubic, exponential TSFs is compared in this section. A 2.3 kW, 6000 rpm, three-phase 12/8 SRM with dc-link voltage 300 V is used for the comparison. The finite element analysis (FEA) of the studied SRM is conducted in JMAG software [30] and the inductance profile and torque profile of studied SRM is shown in Figs. 3(a) and (b), respectively.

Turn-on angle $\theta_{\rm on}$, turn-off angle $\theta_{\rm off}$ and overlapping angle θ_{ov} of linear TSF, cubic TSF, and exponential TSF are set to 5°, 20°, and 2.5°, respectively. Please note that the angles provided in this paper are expressed in mechanical degrees. Torque reference is set to be 1 Nm. Typical waveforms of reference torque, reference current, flux linkage, and ARCFL in terms of rotor position are shown in Fig. 4. Comparison regarding ARCFL of incoming phase and outgoing phase for linear TSF is shown in Fig. 4(e). Based on this comparison, two operational modes (Modes I and II) are clearly noted in this figure. In Mode I, ARCFL of incoming phase is higher; and in Mode II, ARCFL of outgoing phase becomes much higher. Two operational modes are applied to all three types of conventional TSFs. Therefore, the maximum ARCFL is determined by the incoming phase in Mode I and the outgoing phase in Mode II. Since maximum ARCFL at the end of commutation is much larger than that the one at the start of commutation in conventional TSFs, the maximum TRFS is defined by the outgoing phase.

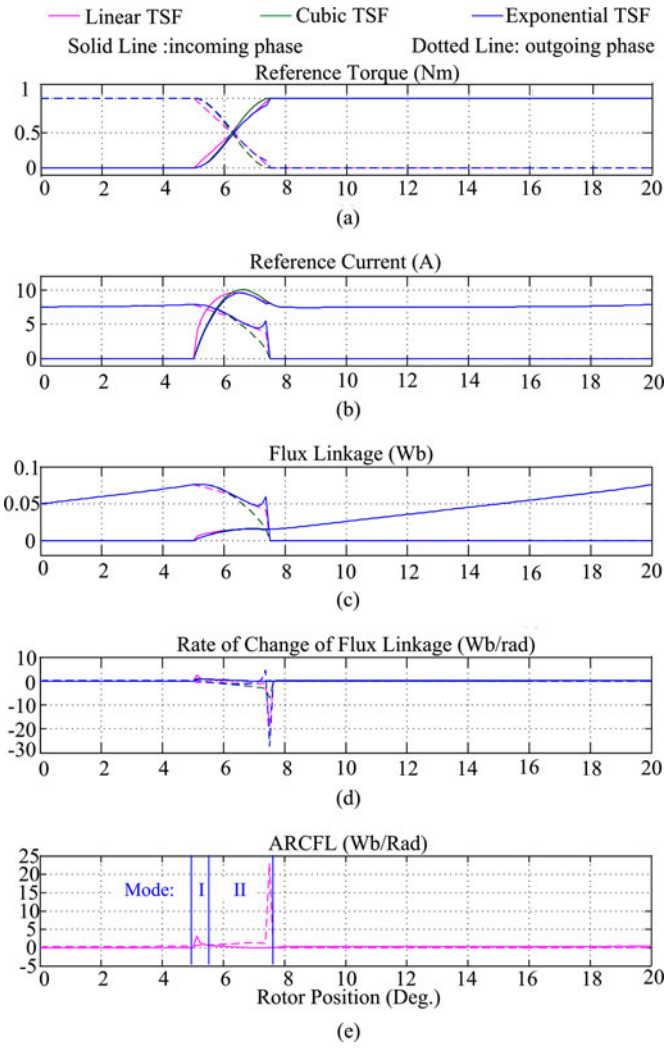

Fig. 4. Torque reference, current reference, flux linkage, and rate of change of flux linkage of conventional TSFs. (a) Reference torque. (b) Reference current. (c) Flux linkage. (d) Rate of change of flux linkage. (e) ARCFL.

B. Proposed Online TSF

Based on the comparison of ARCFL of incoming phase and outgoing phase, two operational modes are introduced and

principles of the proposed online TSF in these modes are explained in this section. The goal of the proposed online TSF is to minimize the maximum ARCFL. The copper loss of online TSF will be compared to conventional TSFs through simulation results.

1) Mode I: As discussed earlier, the ARCFL of outgoing phase is lower than incoming phase at the start of commutation which is denoted as Mode I in Fig. 4. Since ARCFL of the outgoing phase is lower in Mode I, for an ideal case, it can be assumed that the torque of the outgoing phase is equal to its reference

$$T_{e\_\mathrm{ref}(k-1)} = T_{e\_(k-1)}. \tag{12}$$

Torque tracking error ΔT of the incoming phase can be obtained as (13), which could be positive or negative. Adding (12) and (13) together, (14) can be derived. The total torque error is denoted by ΔT, which is introduced by the incoming phase

$$T_{e\_\mathrm{ref}(k)} = T_{e\_(k)} + \Delta T \tag{13}$$

$$T_{e\_\mathrm{ref}} = T_{e\_\mathrm{ref}(k-1)} + T_{e\_\mathrm{ref}(k)} = T_{e\_(k-1)} + T_{e\_(k)} + \Delta T$$
$$\Rightarrow T_{e\_\mathrm{ref}} = T_e + \Delta T. \tag{14}$$

Since the outgoing phase has better tracking performance, its torque reference can be modified as

$$T^{\mathrm{new}}_{e\_\mathrm{ref}(k-1)} = T_{e\_\mathrm{ref}(k-1)} + \Delta T. \tag{15}$$

The torque response of the outgoing phase can be obtained assuming the tracking error of the outgoing phase is zero

$$T^{\mathrm{new}}_{e(k-1)} = T^{\mathrm{new}}_{e\_\mathrm{ref}(k-1)} = T_{e\_\mathrm{ref}(k-1)} + \Delta T. \tag{16}$$

The torque response of the incoming phase is kept the same as (13) since the torque reference of the incoming phase is unchanged. Then, the torque response of incoming phase can be represented as

$$T^{\mathrm{new}}_{e\_(k)} = T_{e\_(k)} = T_{e\_\mathrm{ref}(k)} - \Delta T. \tag{17}$$

By adding (16) and (17) together, the sum of the torque response of incoming phase and outgoing phase are obtained as (18). The torque ripple is eliminated if the tracking error of outgoing phase is zero. Therefore, in Mode I, the torque error is determined by tracking precision of the outgoing phase, which has lower ARCFL

$$\begin{aligned} T^{\mathrm{new}}_{e} &= T^{\mathrm{new}}_{e\_(k)} + T^{\mathrm{new}}_{e\_(k-1)} \\ &= \left(T_{e\_\mathrm{ref}(k)} - \Delta T\right) + \left(T_{e\_\mathrm{ref}(k-1)} + \Delta T\right) \\ &= T_{e\_\mathrm{ref}}. \end{aligned} \tag{18}$$

The control diagram of online TSF is shown in Fig. 5. Only two phases are conducting during commutation. $(k$–$1)$th phase and (k)th phase represents the outgoing phase and incoming phase, respectively. $T\,(\theta, i)$ illustrates the torque equation of the SRM in both linear magnetic and saturated magnetic regions, which can be obtained by either experiment or FEA simulation. $I\,(\theta, T)$ represent the torque to current conversion in both linear magnetic region and saturated magnetic region. If precise

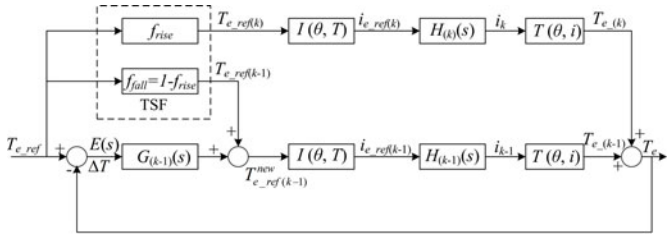

Fig. 5. Control diagram of online TSF in Mode I.

torque–current-angle characteristics of SRM are known, relationship between $I\,(\theta, T)$ and $T\,(\theta, i)$ at the same rotor position θ can be derived as (19). The control diagram in Fig. 5 can be applied to SRM in both linear magnetic and saturated region, since (19) is applicable in both regions

$$I(\theta, T) = \frac{1}{T(\theta, i)}. \tag{19}$$

Transfer functions $H_{(k-1)}(s)$ and $H_{(k)}(s)$ represent current response for outgoing and incoming phases, respectively. Time delay of current control loop is dependent on the rotor position and speed; therefore, an analytical expression is hard to obtain. The maximum time delay of the current control loop is considered to simplify the controller design. $H_{(k-1)}(s)$ and $H_{(k)}(s)$ are denoted as (20) and (21). Maximum time delay is assumed to be 0.001 s both for the incoming and outgoing phases. This maximum time delay can be obtained by simulation, which is dependent on speed and motor parameters

$$H_{(k-1)}(s) = \frac{1}{\tau_1 s + 1} \tag{20}$$

$$H_{(k)}(s) = \frac{1}{\tau_2 s + 1} \tag{21}$$

where τ_1 and τ_2 are time delay of outgoing phase and incoming phase, respectively.

Thus, the currents of each phase are obtained as

$$i_{(k-1)} = \frac{1}{\tau_1 s + 1} i_{\mathrm{ref}\_(k-1)} \tag{22}$$

$$i_{(k)} = \frac{1}{\tau_2 s + 1} i_{\mathrm{ref}\_(k)}. \tag{23}$$

As shown in Fig. 5, online TSF can be regarded as a closed-loop control system, where $G_{(k-1)}(s)$ is the feedback compensator and TSF is regarded as feed-forward compensator. The open-loop transfer function of online TSF can be obtained as

$$\mathrm{TSF}(s) = G_{(k-1)}(s) H_{(k-1)}(s). \tag{24}$$

The torque error transfer function $E(s)$ is defined as (25) and the torque response is represented as

$$E(s) = T_{e\_\mathrm{ref}} - T_e \tag{25}$$

$$T_e = (1 - f_{\mathrm{rise}}) T_{e\_\mathrm{ref}} H_{(k-1)}(s) + f_{\mathrm{rise}} T_{e\_\mathrm{ref}} H_{(k)}(s) + E(s) G_{(k-1)}(s) H_{(k-1)}(s). \tag{26}$$

Combining (24), (25), and (26), the transfer function from reference to error of online TSF can be derived as

$$\frac{E(s)}{T_{e\_\mathrm{ref}}}=\frac{1-(1-f_{\mathrm{rise}})H_{(k-1)}(s)-f_{\mathrm{rise}}H_{(k)}(s)}{1+\mathrm{TSF}(s)}. \quad (27)$$

In case of conventional TSF, since there is no torque error compensation, $G_{(k-1)}(s)$ equals to zero and open-loop transfer function TSF(s) equals to zero. Therefore, the transfer function from reference to error of conventional TSFs is illustrated as

$$\frac{E(s)}{T_{e\_\mathrm{ref}}}=\frac{T_{e\_\mathrm{ref}}-T_e}{T_{e\_\mathrm{ref}}}=1-(1-f_{\mathrm{rise}})H_{(k-1)}(s)-f_{\mathrm{rise}}H_{(k)}(s). \quad (28)$$

By applying online TSF, the torque error is added to the torque reference of outgoing phase to compensate the torque error mainly introduced by the incoming phase in Mode I. Torque reference of the outgoing phase was defined in (15). As shown in Fig. 5, by adding compensator $G_{(k-1)}(s)$, the torque reference of the outgoing phase can be expressed as

$$T^{\mathrm{new}}_{e\_\mathrm{ref}(k-1)}=T_{e\_\mathrm{ref}(k-1)}+\Delta T G_{(k-1)}(s). \quad (29)$$

As compared to (15), $G_{(k-1)}(s)$ in (29) is set to 1. As explained earlier, this is valid for an ideal case where the tracking error of the outgoing phase is assumed to be zero. Thus, the open-loop transfer function TSF(s) of online TSF is equal to $H_{(k-1)}(s)$ as shown in (24). At low frequencies, $H_{(k-1)}(s)$ will be close to one and therefore the open-loop transfer function TSF(s) in (24) will be also close to 1. Now, the transfer function from reference to error of online TSF can be expressed as

$$\frac{E(s)}{T_{e\_\mathrm{ref}}}=\frac{1-(1-f_{\mathrm{rise}})H_{(k-1)}(s)-f_{\mathrm{rise}}H_{(k)}(s)}{2}. \quad (30)$$

Compared to the transfer function for the conventional TSFs in (28), it can be observed that for the same torque reference, torque error of online TSF is reduced by only 50% and therefore the performance of online TSF in torque ripple reduction is still limited.

The parameters of the PI compensator $G_{(k-1)}(s)$ are adjusted to increase the gain of the open-loop transfer function at low frequencies. The crossover frequency is normally selected no larger than one-tenth of the minimum switching frequency. The switching frequency of the studied SRM varies between 10 and 50 kHz, depending on the rotor position and hysteresis band. Therefore, the crossover frequency is selected as about 1 kHz. In order to ensure the stability, phase margin is selected greater than 60°. One possible selection of compensator $G_{(k-1)}(s)$ is shown in (31). The compensator $G_{(k-1)}(s)$ could be later adjusted according to the operation of the motor. Bode plots of $H_{(k-1)}(s)$ and $G_{(k-1)}(s)H_{(k-1)}(s)$ are shown in Fig. 6. The amplitude of open-loop transfer function is greatly enhanced after compensator $G_{(k-1)}(s)$ and thus the torque tracking error can be further reduced

$$G_{(k-1)}(s)=10+\frac{10}{s}. \quad (31)$$

2) Mode II: In Mode II, the ARCFL of incoming phase is lower than that of outgoing phase and therefore the torque error of online TSF is determined by tracking ability of the incoming phase in Mode II. Similarly, the control diagram of online TSF in Mode II is shown in Fig. 7. The compensator of incoming phase $G_{(k)}(s)$ is selected the same as $G_{(k-1)}(s)$.

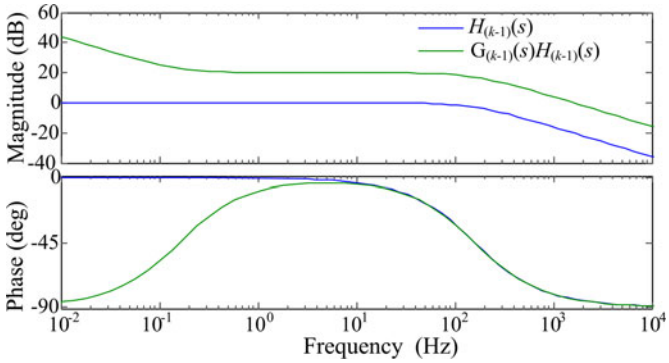

Fig. 6. Bode plot of the open-loop transfer function before and after compensation.

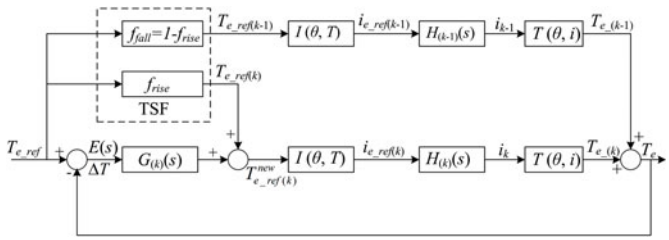

Fig. 7. Control diagram of online TSF in Mode II.

TABLE I
COMPARISON OF THE ONLINE TSFS

Mode I	Mode II
$T_{e\_ref(k)}=f_{rise}(\theta)T_{e\_ref}$	$T_{e\_ref(k)}=f_{rise}(\theta)T_{e\_ref}$
$T_{e\_ref(k-1)}=(1-f_{rise}(\theta))T_{e\_ref}$	$+G_{(k)}(T_{e\_ref}-T_e)$
$+G_{(k-1)}(T_{e\_ref}-T_e)$	$T_{e\_ref(k-1)}=(1-f_{rise}(\theta))T_{e\_ref}$

Comparison of online TSF in Modes I and II is shown in Table I. The compensator based on the torque error is added to the torque reference of the outgoing phase in Mode I, while the compensator is added to the torque reference of the incoming phase in Mode II.

C. Comparison Between Conventional TSFs and Proposed Online TSF

In conventional TSFs, the torque error is determined by the phase with worse tracking ability (higher ARCFL) and therefore the maximum ARCFL M_λ of conventional TSFs is defined as in (8). The torque error of online TSF is determined by the phase with better tracking ability (lower ARCFL) in Modes I and II, and therefore the maximum ARCFL M_λ of the online TSF is defined as

$$M_\lambda=\min\left\{\left|\frac{d\lambda_{\mathrm{rise}}}{d\theta}\right|,\left|\frac{d\lambda_{\mathrm{fall}}}{d\theta}\right|\right\}. \quad (32)$$

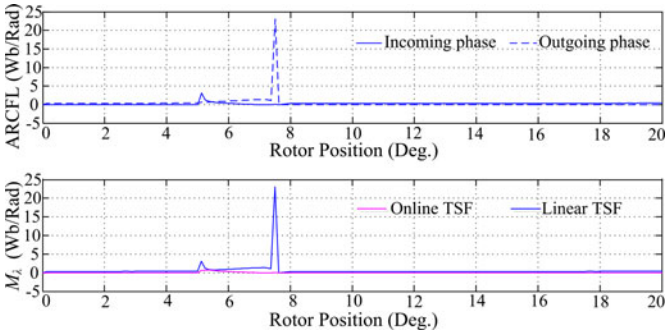

Fig. 8. Comparison of maximum ARCFL of linear TSF and online TSF.

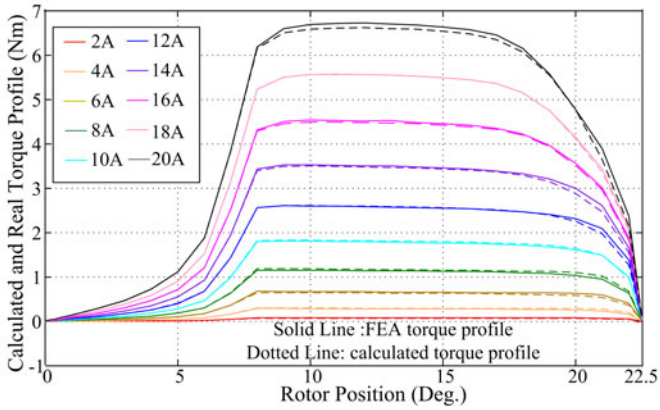

Fig. 9. Comparison of calculated and FEA torque profile.

Comparison of linear TSF and linear-based online TSF is shown in Fig. 8. Torque reference is set to be 1 Nm. The M_λ of linear-based online TSF at the end of commutation is much lower than that of linear TSF. The M_λ of linear-based online TSF, linear TSF, cubic TSF, and exponential TSF is 0.7, 18.8, 7.15, and 27.2 Wb/rad, respectively. Therefore, according to (10), the maximum TRFS of linear-based online TSF, linear TSF, cubic TSF, and exponential TSF are 4194, 152, 400, and 105 rpm, respectively. The maximum TRFS of linear-based online TSF is more than ten times as high as that of the cubic TSF, which has best torque–speed performance among the conventional TSFs. The maximum ARCFL of cubic-based online TSF, exponential-based online TSF, and linear-based online TSF are very similar; therefore, only linear-based online TSF is considered in this paper and from this point forward it will be referred as online TSF. Since torque reference from the online TSF varies at different speeds, the copper loss of online TSF is also a function of speed. Copper loss of online TSF at different speeds will be compared to those of conventional TSFs in the next section through simulation results.

IV. Torque Profile Considering Magnetic Saturation

The torque equation in (1) works in linear magnetic region. In order to extend the proposed online TSF to the saturated magnetic region, torque equation in saturated magnetic region will be presented in this section. In this paper, the torque profile is modeled by using (33), whose details are explained in [25] and [31]

$$T_{ek}(\theta, i) = \frac{a(\theta) i_k^2(\theta)}{(1 + b(\theta) i_k^3(\theta))^{\frac{1}{3}}} \tag{33}$$

where $a\ (\theta)$ and $b\ (\theta)$ are the parameters to be defined as a function of rotor position.

By using curve fitting, parameters $a\ (\theta)$ and $b\ (\theta)$ are obtained to represent the torque profiles. In Fig. 9, the torque profiles by using (33) and torque profiles by using FEA are denoted as the dotted line and solid line, respectively. It can be found that the torque profiles obtained with (33) match with the FEA torque file in different rotor positions and current levels. The current reference can be obtained as (34) by inverting (33)

$$i_k(\theta) = \frac{T_{ek}(\theta, i)}{a(\theta)} \left(\frac{b(\theta)}{2} + \sqrt{\frac{b^2(\theta)}{4} + \left(\frac{a(\theta)}{T_{ek}(\theta, i)}\right)^3} \right)^{\frac{1}{3}}. \tag{34}$$

V. Simulation Verification

The proposed online TSF is compared to conventional TSFs in terms of RMS current, torque ripples, and average torque through simulation results. The 2.3 kW, 6000 rpm, three-phase 12/8 SRM model is implemented in Matlab/Simulink by using torque as well as inductance profiles from FEA as shown in Fig. 3. Hysteresis current control is applied to the current control loop with 0.5 A hysteresis band. Asymmetric power electronic converter is used to simulate SRM operation under 300 V dc-link voltage. The torque ripple $T_{\rm rip}$ is defined as (35). The torque ripples during commutation are named as commutation torque ripples. During one phase conduction, torque ripples still exist due to current ripples from the hysteresis current control. Torque ripples during one phase conduction are named as noncommutation torque ripples

$$T_{\rm rip} = \frac{T_{\max} - T_{\min}}{T_{av}} \tag{35}$$

where $T_{av}, T_{\max}$, and $T_{\min}$ are the average torque, maximum torque, and minimum torque, respectively.

There is a sampling time limitation in the digital implementation of current hysteresis controller, which results in higher current ripples leading to higher torque ripples in any type of TSFs. In addition, since online TSF can be regarded as feedback control system with torque error as the input, with the higher sampling time, the time delay of the input (torque error) is also increased. The control performance of the online TSF is deteriorated due to higher sampling time and torque ripples may be increased for this reason. Therefore, the sampling time becomes an important factor determining the torque ripples of both conventional TSFs and an online TSF.

In simulation, the sampling time $t_{\rm sample}$ is set to 0.1 and 5 μs, respectively. When $t_{\rm sample}$ is set to 0.1 μs, the torque ripples are mostly contributed by the tracking performance of

TSFs rather than higher sampling time and, hence, the tracking performance of the TSFs can be compared more effectively in terms of torque ripple. Then torque references are set to be 1.5 and 3 Nm to analyze the linear and nonlinear operations both at 6000 and 4000 rpm. The switching frequency is between 50 and 10 kHz depending on the speed and current.

Due to the limitation of the digital controller hardware, the sampling time is 5 μs in the experiments. Therefore, the sampling time in simulation is also set to 5 μs so that a fair comparison between the experimental results and simulation results can be conducted. The switching frequency is between 20 and 10 kHz depending on the speed and current. Same operating conditions have been applied with t_{sample} 5 μs, and the effect of sampling time on torque ripples using different TSFs can be investigated by simulation.

A. Simulation Results at 6000 rpm ($T_{\text{ref}} = 1.5\,\text{Nm}, t_{\text{sample}} = 0.1\,\mu\text{s}$)

Fig. 10 shows simulation results of linear, cubic, exponential, and online TSFs at 6000 rpm when the torque reference is 1.5 Nm and sampling time is 0.1 μs. TRFS of conventional TSFs are much lower than 6000 rpm. Therefore, the torque ripples of linear, cubic, and exponential TSFs are significantly increased at 6000 rpm. Due to much higher torque ripples in conventional TSFs, especially negative torque introduced by the outgoing phase, the average torque is decreased. The TRFS of online TSF is about 4000 rpm, which is slightly lower than the maximum speed of SRM. Minor tracking error is produced by applying online TSF and small ripples are generated. Compared with 20% noncommutation torque ripples, the commutation ripples are still small.

B. Simulation Results at 4000 rpm ($T_{\text{ref}} = 3\,\text{Nm}, t_{\text{sample}} = 0.1\,\mu\text{s}$)

Here, torque reference is increased to 3 Nm to verify the application of the proposed online TSF in the magnetic saturation region. Fig. 11 shows simulation results of linear, cubic, exponential and proposed online TSF at 4000 rpm when the torque reference is 3 Nm and sampling time is 0.1 μs. Due to higher rate of flux linkage at higher torque outputs, torque ripples of conventional TSFs are increased compared with those in lower torque output at the same speed. At 4000 rpm, the torque ripples of the proposed online TSF are kept as the minimum (13%) while torque ripples of conventional TSF increase up to 60%. Therefore, the online TSF shows no deteriorated performance when the motor is operating in the magnetic saturated region.

C. Simulation Results at 6000 rpm ($T_{\text{ref}} = 1.5\,\text{Nm}, t_{\text{sample}} = 5\,\mu\,s$)

The sampling time is increased to 5 μs to investigate the effect of the sampling time on torque ripples. Fig. 12 shows simulation results of linear, cubic, exponential and proposed online TSF at 6000 rpm when the torque reference is 1.5 Nm and sampling time is 5 μs. According to simulation results in Fig. 10 for t_{sample} of 0.1 μs, the torque ripples of linear TSF, cubic TSF, exponential TSF, and online TSF at 6000 rpm were around 67%, 74%, 80%,

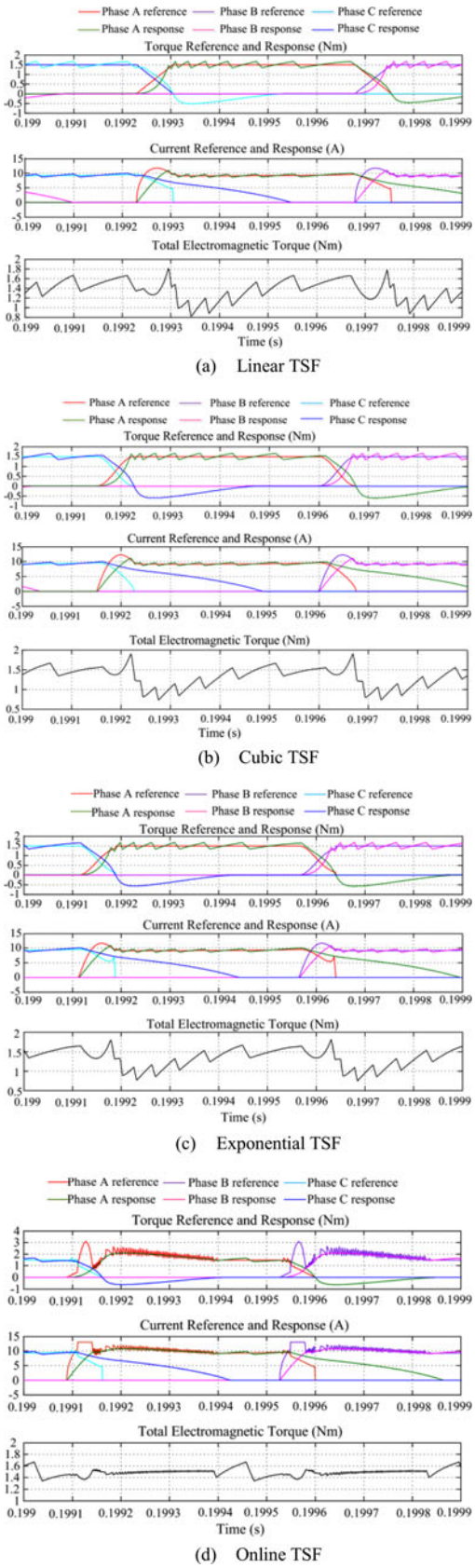

Fig. 10. Simulation results with different TSFs (speed $= 6000\,\text{rpm}, T_{\text{ref}} = 1.5\,\text{Nm}$, and $t_{\text{sample}} = 0.1\,\mu\text{s}$). (a) Linear TSF. (b) Cubic TSF. (c) Exponential TSF. (d) Online TSF.

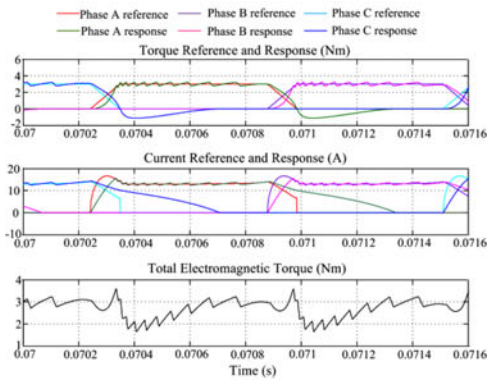

(a) Linear TSF

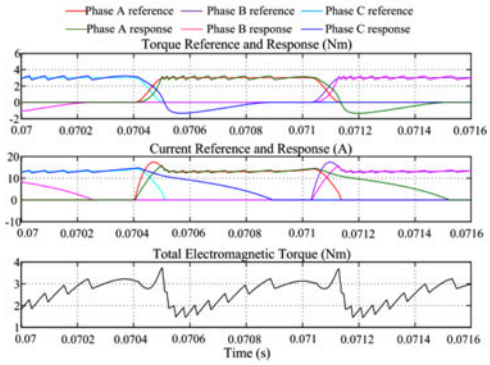

(b) Cubic TSF

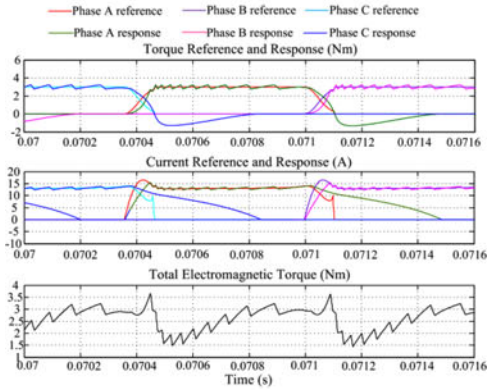

(c) Exponential TSF

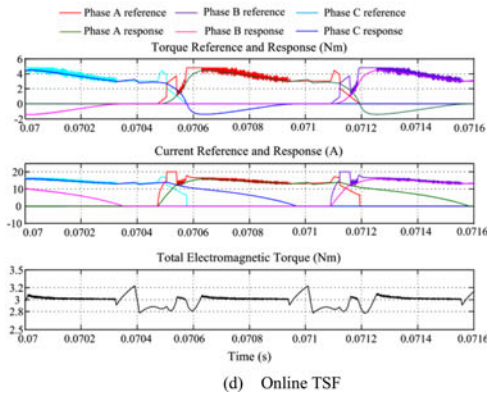

(d) Online TSF

Fig. 11. Simulation results with different TSFs ($\mathrm{speed} = 4000\,\mathrm{rpm}$, $T_{\mathrm{ref}} = 3\,\mathrm{Nm}$, and $t_{\mathrm{sample}} = 0.1\,\mu\mathrm{s}$). (a) Linear TSF. (b) Cubic TSF. (c) Exponential TSF. (d) Online TSF.

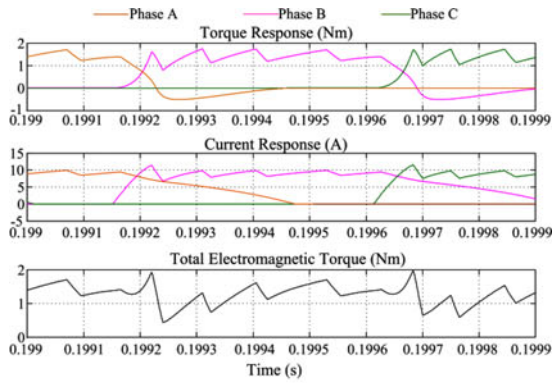

(a) Linear TSF

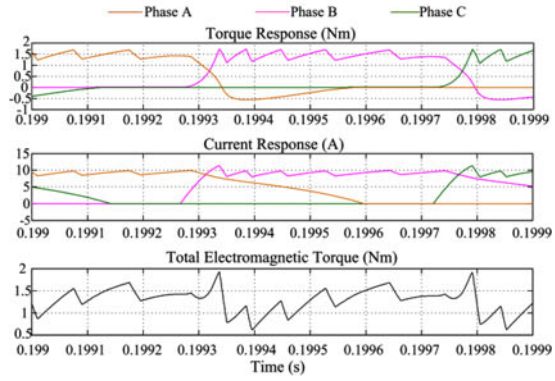

(b) Cubic TSF

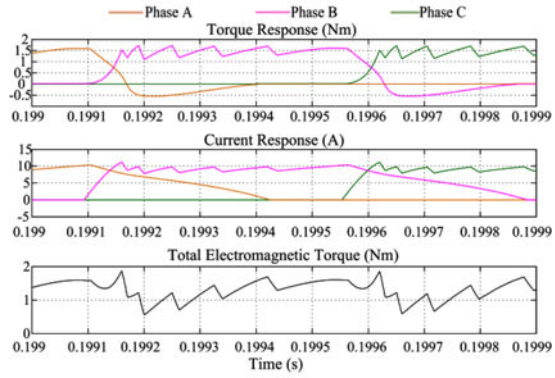

(c) Exponential TSF

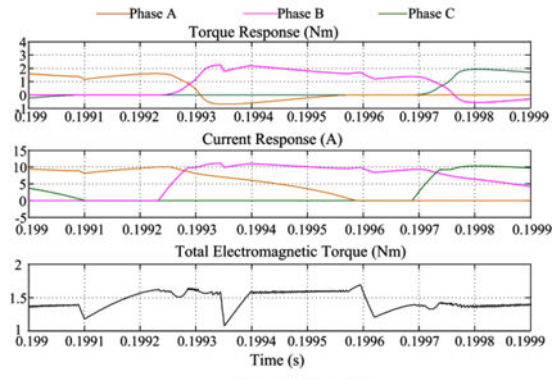

(d) Online TSF

Fig. 12. Simulation results with different TSFs ($\mathrm{speed} = 6000\,\mathrm{rpm}$, $T_{\mathrm{ref}} = 1.5\,\mathrm{Nm}$, and $t_{\mathrm{sample}} = 5\,\mu\mathrm{s}$). (a) Linear TSF. (b) Cubic TSF. (c) Exponential TSF. (d) Online TSF.

and 20%, respectively. As the sampling time is increased to 5 μs, the torque ripples of linear TSF, cubic TSF, exponential TSF and online TSF are increased to 100%, 93%, 80%, and 40%, respectively. With much higher sampling time, torque ripples of TSFs are increased due to current hysteresis controller. Furthermore, due to longer time delay in the feedback control system, the online TSF shows twice torque ripples. However, the online TSF shows one half of torque ripples as the best case in conventional TSFs. Therefore, the online TSF demonstrates better performance in torque ripple reduction compared with conventional TSFs at higher sampling time in linear magnetic region.

D. Simulation Results at 4000 rpm ($T_{\mathrm{ref}} = 3\,\mathrm{Nm}, t_{\mathrm{sample}} = 5\,\mu\mathrm{s}$)

In magnetic saturation region ($T_{\mathrm{ref}} = 3\,\mathrm{Nm}$), the sampling time is increased to 5 μs at 4000 rpm. Fig. 13 shows simulation results of linear, cubic, exponential and proposed online TSF at 4000 rpm when the torque reference is 3 Nm and sampling time is 5 μs. According to the simulation results in Fig. 11 for t_{sample} of 0.1 μs, the torque ripples of linear TSF, cubic TSF, exponential TSF, and online TSF at 4000 rpm were around 67%, 88%, 67%, and 13%, respectively. As the sampling time is increased to 5 μs, the torque ripples of linear TSF, cubic TSF, exponential TSF, and online TSF are 67%, 90%, 88%, and 41%, respectively. Due to higher back EMF at higher current level, the rate of change of phase current is reduced. The influence of the sampling time on current hysteresis controller becomes negligible and therefore no significant changes are observed in torque ripples of conventional TSFs. However, with much higher sampling time, the control performance of the online TSF shows some degree of deterioration such as the fluctuation of the waveforms in the incoming–outgoing region. This leads to much higher commutation torque ripples. However, when the sampling time is 5 μs, the torque ripple of online TSF is still smaller than conventional TSFs in magnetic saturation region.

E. Comparison of Commutation Torque Ripple and RMS Current When the Torque Reference is Set to 1.5 Nm

Torque ripples can be compared more fairly when the sampling time is set to 0.1 μs. In this case, the effect of the sampling time on torque–speed performance of TSFs can be nearly eliminated and the torque ripples of TSFs are mostly contributed by the tracking performance of TSFs. In this section, torque ripples, average torque, RMS current are compared when the sampling time is 0.1 μs. The torque ripple of different TSFs is compared in Fig. 14. The torque ripples of linear, cubic, and exponential TSFs at 6000 rpm are more than three times as high as noncommutation ripples. Below 1000 rpm, cubic TSF shows lower torque ripples than exponential TSF and linear TSF. However, it shows higher torque ripples at higher speed. At 6000 rpm, linear TSF has around 15% lower torque as compared to cubic TSF. The torque ripples of the proposed online TSF are kept constant over a wide speed range and are equal to the noncommutation ripples. Thus, the maximum torque ripple of online TSF is only 25%, 27%, and 30% of that of linear, exponential, and cubic TSFs.

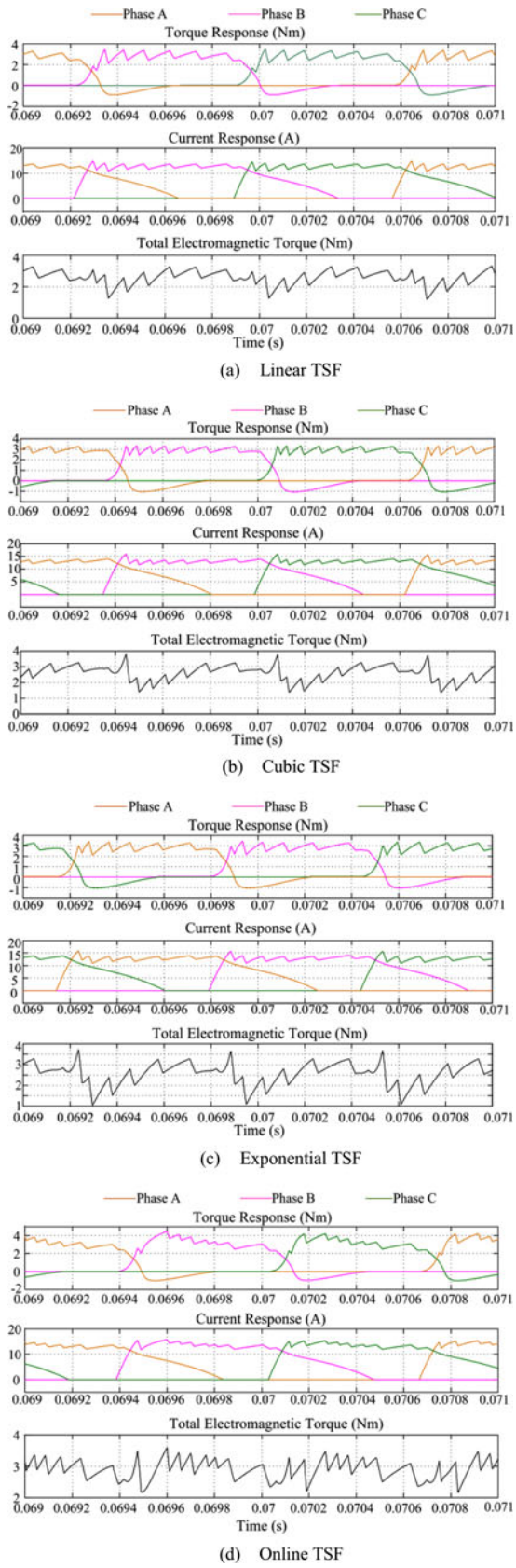

Fig. 13. Simulation results with different TSFs (speed $= 4000\,\mathrm{rpm}, T_{ref} = 3\,\mathrm{Nm}$, and $t_{\mathrm{sample}} = 5\,\mu\mathrm{s}$). (a) Linear TSF. (b) Cubic TSF. (c) Exponential TSF. (d) Online TSF.

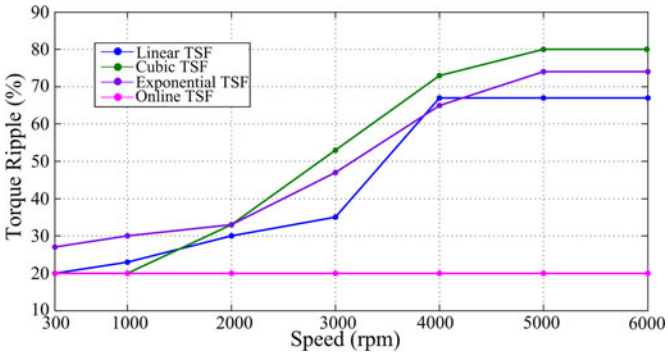

Fig. 14. Comparison of torque ripple of different TSFs ($T_{\rm ref} = 1.5\,{\rm Nm}$ and $t_{\rm sample} = 0.1\,\mu{\rm s}$).

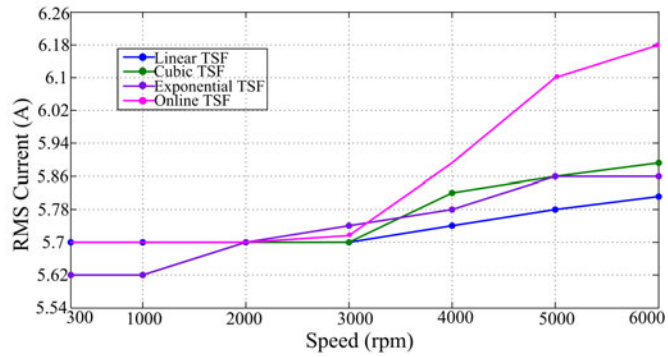

Fig. 15. Comparison of RMS current of different TSFs ($T_{\rm ref} = 1.5\,{\rm Nm}$ and $t_{\rm sample} = 0.1\,\mu{\rm s}$).

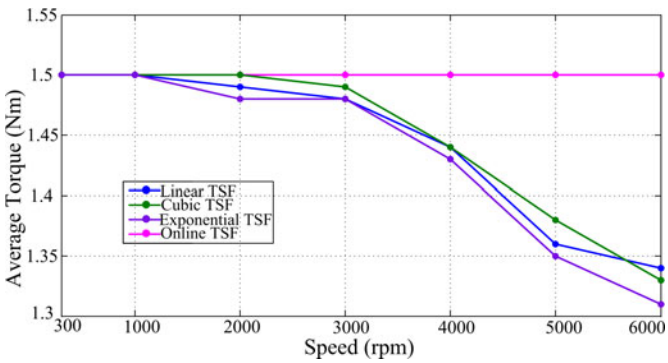

Fig. 16. Comparison of average torque of different TSFs ($T_{\rm ref} = 1.5\,{\rm Nm}$ and $t_{\rm sample} = 0.1\,\mu{\rm s}$).

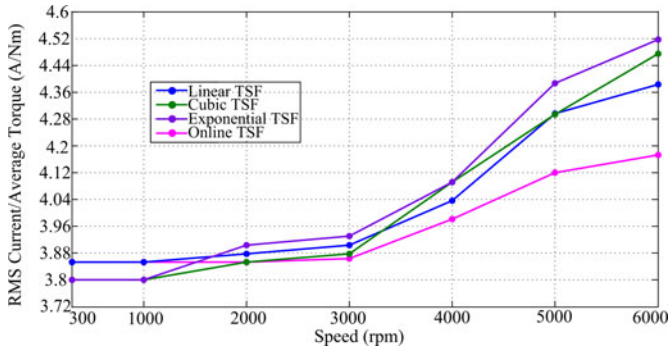

Fig. 17. Comparison of RMS current per average torque of different TSFs ($T_{\rm ref} = 1.5\,{\rm Nm}$ and $t_{\rm sample} = 0.1\,\mu{\rm s}$).

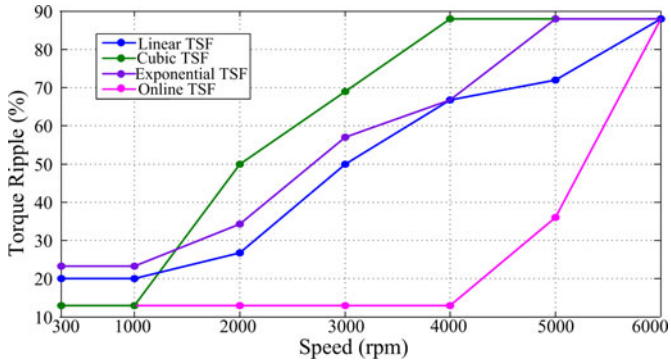

Fig. 18. Comparison of torque ripples of different TSFs ($T_{\rm ref} = 3\,{\rm Nm}$ and $t_{\rm sample} = 0.1\,\mu{\rm s}$).

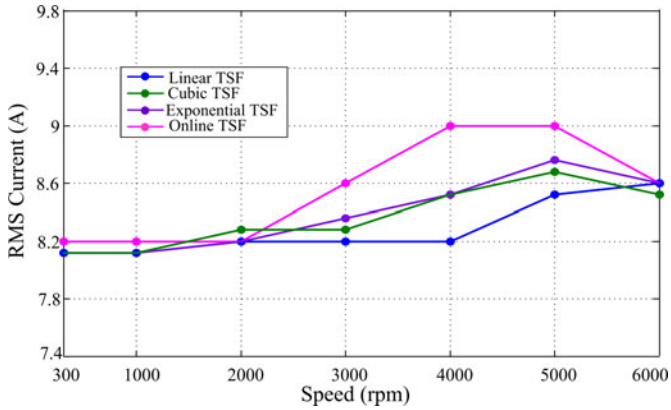

Fig. 19. Comparison of RMS current of different TSFs ($T_{\rm ref} = 3\,{\rm Nm}$ and $t_{\rm sample} = 0.1\,\mu{\rm s}$).

RMS current of different TSFs are compared in Fig. 15. Differences in RMS current for different TSFs are minor and can be neglected below 3000 rpm. At higher speeds, the RMS current of the proposed online TSF shows slight increase. However, as shown in Fig. 16, the average torque of conventional TSFs is decreased as the speed increases.This is due to the poor tracking capability of conventional TSFs. The proposed online TSF has much better tracking capability and it follows the torque reference with much lower commutation torque ripples. Therefore, it should be noted that, due to higher average torque output, RMS current of online TSF is slightly higher.

Online TSF has better tracking capability as compared to other TSFs. In order to match with the same average torque, higher torque reference should be given to other conventional TSFs, which may eventually results in higher RMS current than online TSF. Therefore, the ratio between RMS current and average torque is introduced as (36) in order to compare performance of different TSFs for the same torque reference.This index worksas an operational parameterrather than a design parameter for the motor. Comparison of the ratio between conventional TSFs and online TSF is depicted in Fig. 17. Ratio of online TSF is close to that of conventional TSFs at speeds lower than 2000 rpm and much lower than that of conventional TSFs at higher speed. Therefore, for per unit average torque, online TSF produces equivalent or lower RMS current than

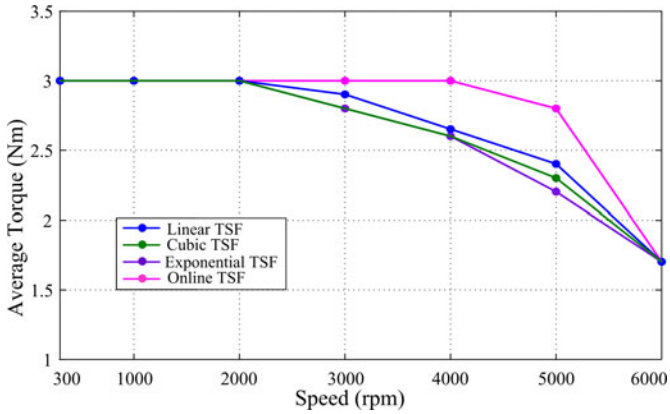

Fig. 20. Comparison of average torque of different TSFs ($T_{\rm ref} = 3\,{\rm Nm}$ and $t_{\rm sample} = 0.1\,\mu{\rm s}$).

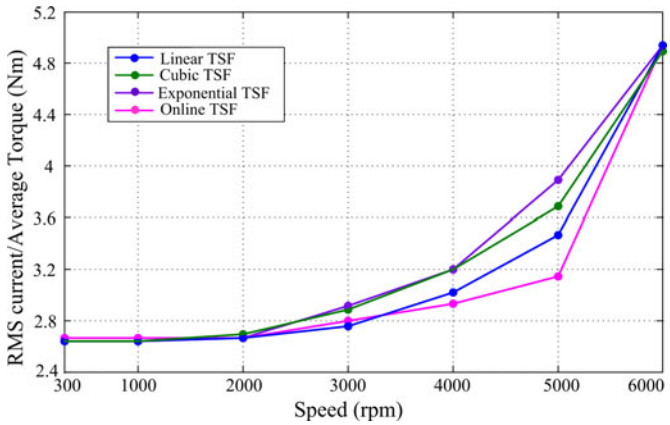

Fig. 21. Comparison of RMS current per average torque of different TSFs ($T_{\rm ref} = 3\,{\rm Nm}$ and $t_{\rm sample} = 0.1\,\mu{\rm s}$).

conventional TSFs, which will not pose challenge on the rating of the motor

$$\text{Ratio} = \frac{I_{\rm RMS}}{T_{av}}. \tag{36}$$

F. Comparison of Commutation Torque Ripple and RMS Current When the Torque Reference is Set to 3 Nm

The analysis on the performance of TSFs in magnetic saturation region, the sampling time is also set to 0.1 μs to eliminate sampling time effect. Torque ripple, RMS current, average torque and RMS current per average torque of different TSFs are compared in Figs. 18–21 when the torque reference is set to 3 Nm. Online TSF shows no obvious increase in torque ripples as the speed increases, while, the torque ripples of conventional TSFs are greatly increased below 4000 rpm. At speeds higher than 5000 rpm, the current control capability of the SRM reduces and, hence, all TSFs show similar torque ripples. Among the three conventional TSFs, linear TSF shows the minimum torque ripples at 4000 rpm, which are still five times as high as online TSF. Compared with conventional TSFs, online TSF shows slightly higher RMS current, higher average torque, and lower RMS current per average torque over the wide speed range. Therefore, in magnetic saturation region, the online TSF is more effective than conventional TSFs in terms of torque ripple reduction.

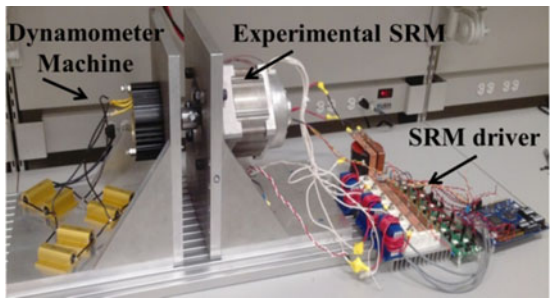

Fig. 22. Experimental setup of SRM drive.

VI. Experimental Results

The proposed online TSF is verified in a 2.3 kW, 6000 rpm, three-phase 12/8 SRM shown in Fig. 22. FPGA EP3C25Q240 is used for digital implementation of the proposed TSF. Current hysteresis band is set to be 0.5 A, and dc-link voltage is set to 300 V. The sampling time of the digital controller in the experimental setup is set to 5 μs. In the experiment, the speed of the motor is between 4000 and 6000 rpm. The switching frequency is between 20 and 10 kHz depending on the speed and torque. As verified with the simulation results previously, higher current ripples and torque ripples can be observed when the sampling time is set to 5 μs rather than 0.1 μs. Similarly, the experimental SRM is operating in two different operating conditions: 1) $T_{\rm ref} = 1.5\,{\rm Nm}, {\rm speed} = 6000\,{\rm rpm}, {\rm t\_sample} = 5\,\mu{\rm s}$ 2) $T_{\rm ref} = 3\,{\rm Nm}, {\rm speed} = 4000\,{\rm rpm},$ and $t_{\rm sample} = 5\,\mu{\rm s}$. Experimental results will be compared with simulation results at the same torque reference, the same speed, and the same sampling time. The torque–current-rotor position characteristics are stored as look up tables in FPGA. Torque is estimated from these look-up tables by measuring the phase current and rotor position, and converted into an analog signal through digital-to-analog conversion chip in the hardware. It should be noted that the torque output of each phase could be negative, since the selected digital-to-analog conversion chip is unipolar. Thus, 2 Nm offset is added to the torque out of each phase in the next a couple of figures and no offset is added to the total torque. The torque reference of online TSF is adjusted online according to the error between the torque reference and estimated torque.

A. Experimental Results at 6000 rpm ($T_{\rm ref} = 1.5\,{\rm Nm}, t_{\rm sample} = 5\,\mu{\rm s}$)

The torque reference is set to 1.5 Nm and sampling time is 5 μs in this experiment. Figs. 23(a) and (b) shows the torque response and current response of linear TSF at 6000 rpm, respectively. Figs. 24(a) and (b) shows the torque response and current response of cubic TSF at 6000 rpm, respectively. Figs. 25(a) and (b) shows the torque response and current response of exponential TSF at 6000 rpm, respectively. Figs. 26(a) and (b) shows the torque response and current response of *online* TSF at 6000 rpm, respectively. The torque ripples of linear TSF, cubic TSF, and exponential TSF at 6000 rpm is around 93%, 102%, 100%, and

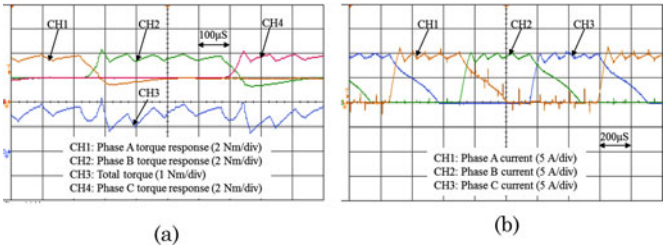

Fig. 23. Experimental results of linear TSF (speed $= 6000\,\mathrm{rpm}$ and $T_{\mathrm{ref}} = 1.5\mathrm{Nm}$). (a) Torque. (b) Current.

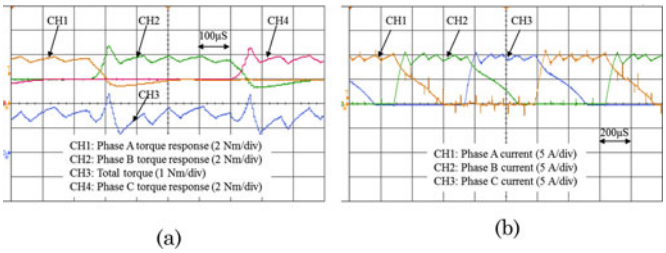

Fig. 24. Experimental results of cubic TSF (speed $= 6000\,\mathrm{rpm}$ and $T_{\mathrm{ref}} = 1.5\mathrm{Nm}$). (a) Torque. (b) Current.

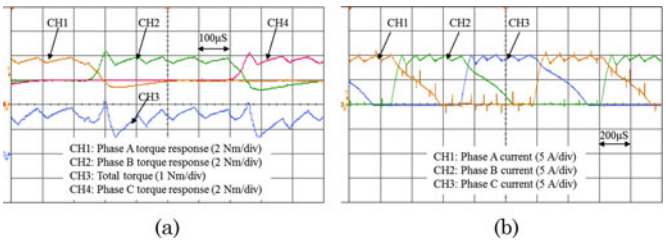

Fig. 25. Experimental results of exponential TSF (speed $= 6000\,\mathrm{rpm}$ and $T_{\mathrm{ref}} = 1.5\mathrm{Nm}$). (a) Torque. (b) Current.

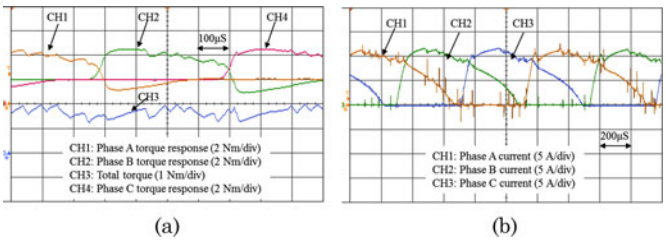

Fig. 26. Experimental results of online TSF (speed $= 6000\,\mathrm{rpm}$ and $T_{\mathrm{ref}} = 1.5\mathrm{Nm}$). (a) Torque. (b) Current.

40%, compared to 100%, 93%, 80%, and 40% torque ripples in simulation results in Fig. 11. In the experiment, the online TSF produces less than one half of torque ripples of the best case in conventional TSFs, which matches the simulation results in terms of torque ripples, torque response, and current waveforms at the same operation condition. Online TSF has better torque–speed performance than conventional TSFs in linear magnetic region by experimental results.

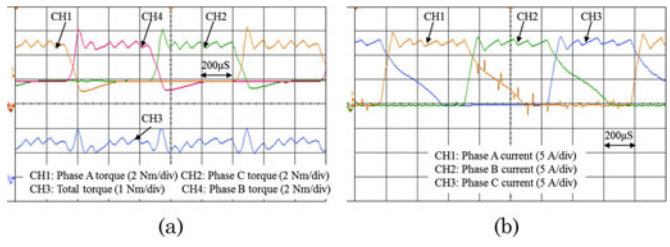

Fig. 27. Experimental results of linear TSF (speed $= 4000\,\mathrm{rpm}$ and $T_{\mathrm{ref}} = 3\mathrm{Nm}$). (a) Torque. (b) Current.

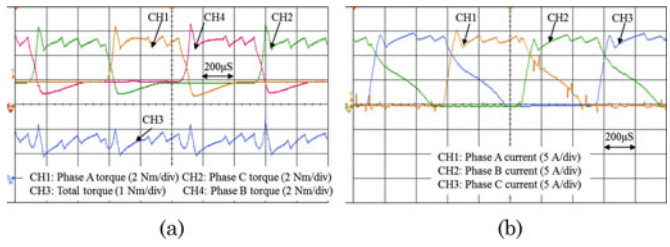

Fig. 28. Experimental results of cubic TSF (speed $= 4000\,\mathrm{rpm}$ and $T_{\mathrm{ref}} = 3\mathrm{Nm}$). (a) Torque response. (b) Current response.

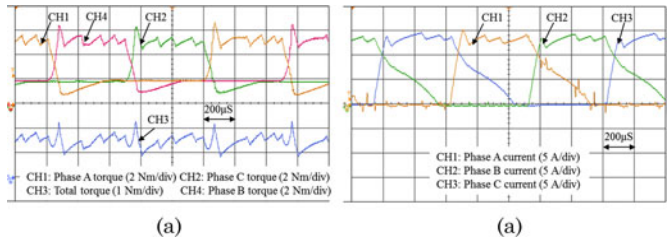

Fig. 29. Experimental results of exponential TSF (speed $= 4000$ rpm and $T_{\mathrm{ref}} = 3\mathrm{Nm}$). (a) Torque. (b) Current.

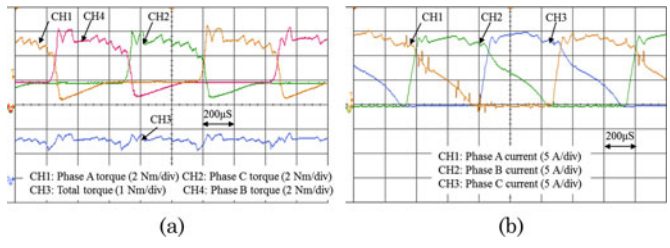

Fig. 30. Experimental results of online TSF (speed $= 4000\,\mathrm{rpm}$ and $T_{\mathrm{ref}} = 3\mathrm{Nm}$). (a) Torque. (b) Current.

B. Experimental Results at 4000 rpm ($T_{\mathrm{ref}} = 3\mathrm{Nm}, t_{\mathrm{sample}} = 5\,\mu\mathrm{s}$)

In this experiment, the torque reference is increased to 3 Nm to verify the performance of online TSF in the magnetic saturated region. The sampling time is still set to 5 μs. Figs. 27(a) and (b) shows the torque response and current response of linear TSF at 4000 rpm, respectively. Figs. 28(a) and (b) shows the torque response and current response of cubic TSF at 4000 rpm, respectively. Figs. 29(a) and (b) shows the torque response and current response of exponential TSF at 4000 rpm, respectively. Figs. 30(a) and (b) shows the torque response and current response of online TSF at 4000 rpm, respectively. Simulation results ($T_{\mathrm{ref}} = 3\,\mathrm{Nm}$, speed $= 4000\,\mathrm{rpm}$, and $t_{\mathrm{sample}} = 5\,\mu\mathrm{s}$)

in Fig. 13 show that the torque ripples of linear TSF, cubic TSF, exponential TSF, and online TSF are 67%, 90%, 88%, and 41%, respectively. Experimental results shown in Figs. 27–30 show that the torque ripples of linear TSF, cubic TSF, and exponential TSF are increased to up to 67%, 83%, and 93%, and 40%. Therefore, experimental results of different TSFs are close to the simulation results in terms of torque ripples, torque response, and current waveforms when sampling time, torque reference, and speed of the motor are the same. The application of online TSF in magnetic saturation region is verified by this experiment.

VII. Conclusion

In this paper, an extended-speed low-ripple torque control of SRM drives using TSF is presented. Two operational modes of online TSF are defined. In mode I, ARCFL of incoming phase is higher than outgoing phase, and in mode II, ARCFL of outgoing phase is higher than incoming phase. PI compensator with the error between the estimated torque and torque reference is added to the torque reference of the outgoing phase in Mode I and the incoming phase in Mode II.

With a 2.3 kW, 6000 rpm, three-phase 12/8 SRM, the maximum TRFS of the proposed online TSF is increased to about 4000 rpm, which is more than ten times as high as the best case in these conventional TSFs. The online TSF is compared to conventional TSFs in terms of torque ripple, RMS current, average torque, and RMS current per average torque through simulation results. The torque ripples of TSFs are influenced by the sampling time due to digital implementation of hysteresis controller or time delay of feedback control system. With the lower sampling time, the torque ripples are mostly contributed by the tracking performance of TSFs. The simulation results at lower sampling time show that in linear magnetic torque region, online TSF only produces 25%, 27%, and 30% of torque ripples of linear TSF, exponential TSF and cubic TSF, respectively. In order to extend the application of online TSF to magnetic saturated region, the nonlinear torque profiles in terms of rotor position and current are obtained. When the torque reference is 3 Nm, the online TSF produces around one-fifth of the maximum torque ripples compared with conventional TSFs in chopping mode. Constant torque range of online TSF is extended to 4000 rpm compared with 2000 rpm in conventional TSFs accordingly. In addition, due to its better tracking capability, online TSF generates higher average torque for the given torque reference as compared to conventional TSFs. This results in slightly higher RMS current. However, for per unit average torque, the RMS current of online TSF is not increased, which will not influence power rating of the motor.

The performance of online TSF is compared to conventional TSFs by an experimental a 2.3 kW, 6000 rpm, three-phase 12/8 SRM. Both simulation results and experimental results prove that the online TSF is a promising candidate for torque ripple reduction over the wide speed range.

Acknowledgment

This research was undertaken, in part, thanks to funding from the Canada Excellence Research Chairs Program.

References

[1] K Krishnan, *Switched Reluctance Motor Drives: Modeling, Simulation, Analysis, Design, and Applications*. Boca Raton, FL,USA: CRC Press, Jun. 2001.

[2] T. J. E. Miller, *Electronic Control of Switched Reluctance Machines*. New York, NY, USA: Reed Educational and Professional, 2001.

[3] M. Krishnamurthy, C. S. Edrington, A. Emadi, P. Asadi, M. Ehsani, and B. Fahimi, "Making the case for applications of switched reluctance motor technology in automotive products," *IEEE Trans. Power Electron.*, vol. 21, no. 3, pp. 659–675, May 2006.

[4] P. C. Desai, M. Krishnamurthy, N. Schofield, and A. Emadi, "Novel switched reluctance machine configuration with higher number of rotor poles than stator poles: concept to implementation," *IEEE Trans. Ind. Electron.*, vol. 57, no. 2, pp. 649–659, Feb. 2010.

[5] P. Shamsi and B. Fahimi, "Single-bus star-connected switched reluctance drive," *IEEE Trans. Power Electron.*, vol. 28, no. 12, pp. 5578–5587, Dec. 2013.

[6] B. Bilgin, A. Emadi, and M. Krishnamurthy, "Design consideration for switched reluctance machines with higher number of rotor poles," *IEEE Trans. Ind. Electron.*, vol. 59, no. 10, pp. 3745–3756, Apr. 2012.

[7] B. Bilgin, A. Emadi, and M. Krishnamurthy, "Comprehensive evaluation of the dynamic performance of a 6/10 SRM for traction application in PHEVs," *IEEE Trans. Ind. Electron.*, vol. 60, no. 7, pp. 2564–2575, Jul. 2013.

[8] X. Cao, Z. Deng, G. Yang, and X. Wang, "Independent control of average torque and radial force in bearingless switched-reluctance motors with hybrid excitations," *IEEE Trans. Power Electron.*, vol. 24, no. 5, pp. 1376–1385, May 2009.

[9] J. Ye, B. Bilgin, and A. Emadi, "Comparative evaluation of power converters for 6/4 and 6/10 switched reluctance machines," in *Proc. IEEE Transp. Electrification Conf. Expo.*, 2012, Dearborn, MI, USA, pp. 1–6.

[10] B. M. Shao and A. Emadi, "A digital PWM control of switched reluctance motor drives," in *Proc. IEEE Veh. Power Propulsion*, 2010, Lille, France, pp. 1–6.

[11] J. Cai and Z. Deng, "Sensorless control of switched reluctance motor based on phase inductance vectors," *IEEE Trans. Power Electron.*, vol. 27, no. 7, pp. 3410–3423, Jul. 2012.

[12] M. D. Hennen, M. Niessen, C. Heyers, H. J. Brauer, and R. W. De Doncker, "Development and control of an integrated and distributed inverter for a fault tolerant five-phase switched reluctance traction drive," *IEEE Trans. Power Electron.*, vol. 27, no. 2, pp. 547–554, Feb. 2012.

[13] C. L. Tseng, S. Y. Wang, S. C. Chien, and C. Y. Chang, "Development of a self-tuning TSK-fuzzy speed control strategy for switched reluctance motor," *IEEE Trans. Power Electron.*, vol. 27, no. 4, pp. 2141–2152, Apr. 2012.

[14] H. Torkaman and E. Afjei, "Comprehensive detection of eccentricity fault in switched reluctance machines using high-frequency pulse injection," *IEEE Trans. Power Electron.*, vol. 28, no. 3, pp. 1382–1390, Mar. 2013.

[15] J. H. Lee, Z. G. Lee, and J. W. Ahn, "Design and operation characteristics of four-two pole high-speed SRM for torque ripple reduction," *IEEE Trans. Ind. Electron.*, vol. 60, no. 9, pp. 3637–3643, Sep. 2013.

[16] J. Kim, K. Ha, and R. Krishnan, "Single-controllable-switch-based switched reluctance motor drive for low cost, variable-speed applications," *IEEE Trans. Power Electron.*, vol. 27, no. 1, pp. 379–387, Jan. 2012.

[17] R. Mikail, I. Husain, Y. Sozer, M. Islam, and T. Sebastian, "Four-quadrant torque ripple minimization of switched reluctance machine through current profiling with mitigation of rotor eccentricity problem and sensor errors," in *Proc. IEEE Energy Convers. Cong. Expo.*, 2012, USA Raleigh, NC, pp. 838–842.

[18] R. Mikail, I. Husain, Y. Sozer, M. Islam, and T. Sebastian, "Torque-ripple minimization of switched reluctance machines through current profiling," *IEEE Trans. Ind. Appl.*, vol. 49, no. 3, pp. 1258–1267, May/Jun. 2013.

[19] S. K. Sahoo, S. Dasgupta, S. K. Panda, and J. Xu, "A Lyapunov function based robust direct torque controller for a switched reluctance motor drive system," *IEEE Trans. Power Electron.*, vol. 27, no. 2, pp. 555–564, Feb. 2012.

[20] I. Husain and S. Hossain, "Modeling, simulation, and control of switched reluctance motor drives," *IEEE Trans. Ind. Electron.*, vol. 52, no. 6, pp. 1625–1634, May 2005.

[21] I. Husain, "Minimization of torque ripple in SRM drive," *IEEE Trans. Ind. Electron.*, vol. 49, no. 1, pp. 28–39, Feb. 2002.

[22] J. F. Pan, N. C. Cheung, and Z. Yu, "An improved force distribution function for linear switched reluctance motor on force ripple minimization

with nonlinear inductance modeling," *IEEE Trans. Magn.*, vol. 48, no. 11, pp. 3064–3067, Nov. 2012.
[23] H. J. Brauer, M. D. Hennen, and R. W. De Doncker, "Control for poly phase switched reluctance machines to minimize torque ripple and decrease ohmic machine losses," *IEEE Trans. Power Electron.*, vol. 27, no. 1, pp. 370–378, Feb. 2012.
[24] X. D. Xue, K. W. E. Cheng, and S. L. Ho, "Optimization and evaluation of torque sharing function for torque ripple minimization in switched reluctance motor drives," *IEEE Trans. Power Electron.*, vol. 24, no. 9, pp. 2076–2090, Sep. 2009.
[25] V. P. Vujiččić, "Minimization of torque ripple and copper losses in switched reluctance drive," IEEE Trans. Power Electron., vol. 27, no. 1, pp. 388–399, Jan. 2012.
[26] D. H. Lee, Z. G. Lee, and J. W. Ahn, "A simple nonlinear logical torque sharing function for low-torque ripple SR Drive," *IEEE Trans. Ind. Electron.*, vol. 56, no. 8, pp. 3021–3028, Aug. 2009.
[27] S. K. Sahoo, S. K. Panda, and J. Xu, "Indirect torque control of switched reluctance motors using iterative learning control," *IEEE Trans. Power Electron.*, vol. 20, no. 1, pp. 200–208, Jan. 2005.
[28] S. K. Sahoo, S. K. Panda, and J. Xu, "Iterative learning-based high-performance current controller for switched reluctance motors," *IEEE Trans. Energy Convers.*, vol. 19, no. 3, pp. 491–498, Sep. 2004.
[29] N. Chayopitak, R. Pupadubsin, and K. Tungpimolrut, "An online low-ripple torque control of switched reluctance motor for small electric vehicle," in *Proc. Int. Conf. Elect. Machines Syst.*, 2008, Wuhan, China, pp. 3327–3332.
[30] JSOL Corporation, JMAG. Application Note.(2013). [Online]. Available: http://www.jmag-international.com/
[31] V. P. Vujicic, "Modeling of a switched reluctance machine based on the invertible torque function," *IEEE Trans. Magn.*, vol. 44, no. 9, pp. 2186–2194, Sep. 2008.

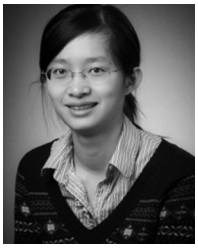

Jin Ye (S'13) received the B.S. and M.S. degrees in electrical engineering from Xi'an Jiaotong University, China, in 2008 and 2011, respectively. She is currently working toward the Ph.D. degree at McMaster Institute for Automotive Research and Technology at McMaster University, Hamilton, ON, Canada.

Her main research interests include battery management systems, digital control of power electronics and electric machines.

Berker Bilgin (S'09–M'12) received the Ph.D. degree in electrical engineering from Illinois Institute of Technology in Chicago, Chicago, IL, USA.

He is the Senior Principle Research Engineer in Canada Excellence Research Chair in Hybrid Powertrain Program in McMaster Institute for Automotive Research and Technology at McMaster University in Hamilton, ON, Canada. He is managing many multidisciplinary projects on the design of electric machines, power electronics, electric motor drives, and electrified powertrains. He is in the organizing committee of the IEEE Transportation Electrification Conference and Expo.

Dr. Bilgin is also serving as an Editor for the IEEE TRANSPORTATION ELECTRIFICATION NEWSLETTER.

Ali Emadi (S'98–M'00–SM'03–F'13) received the B.S. and M.S. degrees in electrical engineering with highest distinction from Sharif University of Technology, Tehran, Iran, in 1995 and 1997, respectively, and the Ph.D. degree in electrical engineering from Texas A&M University, College Station, TX, in 2000.

He is the Canada Excellence Research Chair in Hybrid Powertrain and Director of McMaster Institute for Automotive Research and Technology at McMaster University in Hamilton, ON, Canada. Before joining McMaster University, he was the Harris Perlstein Endowed Chair Professor of Engineering and Director of the Electric Power and Power Electronics Center and Grainger Laboratories at Illinois Institute of Technology (IIT) in Chicago, IL, USA. In addition, he was the Founder, Chairman, and President of Hybrid Electric Vehicle Technologies, Inc. (HEVT)—a university spin-off company of IIT.

Dr. Emadi is the recipient of numerous awards and recognitions. He was the advisor for the Formula Hybrid Teams at IIT and McMaster University, which won the GM Best Engineered Hybrid Systems Award at the 2010 and 2013 competitions, respectively. He is the principal author/coauthor of more than 300 journal and conference papers as well as several books including Vehicular Electric Power Systems (2003), Energy Efficient Electric Motors (2004), Uninterruptible Power Supplies and Active Filters (2004), Modern Electric, Hybrid Electric, and Fuel Cell Vehicles, Second Edition (2009), and Integrated Power Electronic Converters and Digital Control (2009). He is also the editor of the Handbook of Automotive Power Electronics and Motor Drives (2005). He was the inaugural general chair of the 2012 IEEE Transportation Electrification Conference and Expo and has chaired several IEEE and SAE conferences in the areas of vehicle power and propulsion.